ADVANCED ENERGY MATERIALS
www.advenergymat.de

From Sunrise to Sunset: Unraveling Metastability in Perovskite Solar Cells by Coupled Outdoor Testing and Energy Yield Modelling

Marko Remec, Špela Tomšič, Mark Khenkin, Quiterie Emery, Jinzhao Li, Florian Scheler, Boštjan Glažar, Marko Jankovec, Marko Jošt, Eva Unger, Steve Albrecht, Rutger Schlatmann, Benjamin Lipovšek,* Carolin Ulbrich, and Marko Topič*

Perovskite-based solar cells exhibit peculiar outdoor performance which is not yet fully understood. The results of outdoor tests may contain hidden, but valuable information that cannot be fully extracted from measurements alone. One such phenomenon is the effect of nighttime degradation and the subsequent light-soaking recovery, which can take from a few hours in the morning up to the entire day. In this work, long-term outdoor monitoring is combined with energy yield modeling to qualitatively and quantitatively investigate the effect of light-soaking recovery in both single junction and tandem perovskite-based devices. Following the novel methodology presented in this study, it is observed that the light-soaking effect depends not only on the daily irradiation but also on the device temperature, and it can be described using a simple empirical formalism. Incorporating this dependency into the energy yield model results in an excellent agreement between the simulated and the measured outdoor data, which allows to perform long-term prediction studies. The model estimates that the light-soaking metastability effect decreases the attainable annual energy yield by up to ≈5% for the studied single junction devices, and for tandems by up to ≈3%, depending on the geographical location, and even more for non-optimal device orientation.

1. Introduction

The field of photovoltaic (PV) has experienced nearly exponential growth in recent years and the practical power conversion efficiency (PCE) limits of conventional single-junction silicon solar cells will soon be reached.[1] Further progress in the field can be achieved by utilizing emerging halide perovskite-based solar cells (PSCs). In both configurations – single junction (SJ) and tandem with a silicon (or other low-bandgap) bottom cell – the PCEs have already reached levels that are viable for commercialization,[1,2] and keep increasing due to the intense research activities in this field. Device operational stability remains a concern, but a lot of promising development has been demonstrated recently,[3,4] giving grounds for optimism. An important next step in technology development is uncovering the device outdoor stability through field testing, hand in hand with accelerated indoor lifetime testing, and evaluating the long-term production of (area-normalized) electrical energy — the energy yield (EY; given in kWh m^{-2}) – under realistic conditions rather than the PCE under standard test conditions (STC, i.e., 25 °C, 1000 W m^{-2}, AM1.5G spectrum).

The first long-term outdoor datasets with in-situ monitoring of perovskite solar cells[5–7] and tandems with silicon,[8–9] were published in recent years. They show the importance of the reversible (or metastable) processes that result in periodic changes in the efficiency of PSCs during the day-night cycle.[10] One of these phenomena is the so-called light-soaking effect (LSE), i.e., the process of nighttime degradation and subsequent performance recovery upon illumination, typically in the morning hours of the day. The duration of the light-induced recovery can take from minutes[11] up to dozens[12] of hours and strongly depends on the device architecture. It was also shown to increase in magnitude with the device ageing,[13] potentially becoming much more of a problem for aged cells even if they did not show the LSE initially in their fresh state. The physical origin of the LSE in PSCs is still under investigation.[14] The most common explanations involve ion

M. Remec, M. Khenkin, Q. Emery, J. Li, F. Scheler, E. Unger, S. Albrecht, R. Schlatmann, C. Ulbrich
Solar Energy Division
Helmholtz-Zentrum Berlin für Materialien und Energie
12489 Berlin, Germany
E-mail: mark.khenkin@helmholtz-berlin.de
M. Remec, Š. Tomšič, F. Scheler, B. Glažar, M. Jankovec, M. Jošt, B. Lipovšek, M. Topič
Faculty of Electrical Engineering
Laboratory of Photovoltaics and Optoelectronics
University of Ljubljana
Tržaška cesta 25, Ljubljana 1000, Slovenia
E-mail: benjamin.lipovsek@fe.uni-lj.si

The ORCID identification number(s) for the author(s) of this article can be found under https://doi.org/10.1002/aenm.202304452

DOI: 10.1002/aenm.202304452

migration[15–17] trapping/detrapping of charge carriers,[18,19] defects healing,[20,21] and perovskite lattice expansion and strain relaxation[22–24] The LSE not only poses a technical challenge for accurate device characterization but also results in the underperformance of PSCs outdoors for a certain time in the morning. The difference in morning and afternoon efficiency affects single-cell devices and also perovskite modules.[25] The exact quantification of LSE during field testing is challenging due to the constantly changing outdoor conditions. We will demonstrate, however, that state-of-the-art energy yield modelling can be harnessed as a powerful tool for LSE extraction and evaluation.

Multiple EY models were suggested for perovskite-based solar cells[26–29] They vary in complexity, depending on the parameters taken into account by the model (irradiance, temperature, solar spectrum, and solar cell electrical performance among others). The purpose of the models was mainly to predict and optimize EY at different geographical locations,[29] to compare 2-terminal and 4-terminal tandem devices,[30] or to improve light management by analyzing the effects of textured surfaces.[31] To the best of our knowledge, however, no connection with actual outdoor data has been established so far for the purpose of device characterization, which – as we will show – is in fact one of the most powerful uses of energy yield modelling. Namely, when studying the impact of nighttime degradation and light-soaking recovery, it is difficult (if not impossible) to isolate and quantitatively evaluate the extent of the LSE solely from outdoor measurements due to the constantly changing weather conditions. However, by comparing the measured data to the simulated reference device performance unhindered by the LSE, we can quantify the energy harvesting deficit associated with metastability in real time under any given weather and installation conditions. And finally, if the simulation model itself is extended by factoring in the observed metastability, long-term forecasting also becomes possible, and assessment of the EY losses associated with the LSE can be performed on an annual level.

In this work, we performed long-term outdoor tracking of several PSCs and perovskite-silicon (PK-Si) tandem cells at two geographical locations, in Berlin (Germany) and Ljubljana (Slovenia). The selected devices that were monitored for up to 2 years exhibit decent long-term outdoor stability, yet are also subjected to the peculiar diurnal behavior associated with the light-soaking effect, where the devices degrade over the night and then recover significantly from morning to noon or evening, depending on the weather conditions. By simulating the expected device output using an in-house developed energy yield model, we obtain good matching between the model predictions and the outdoor measurements in the evening hours. However, we systematically observe devices underperforming in the mornings, especially when comparing the simulated and the measured voltage at the maximum power point (V_{MPP}), which we attribute to the LSE. From the extent of this difference, the energy losses associated with the observed metastability phenomenon are extracted, quantified, and empirically correlated with the dose of irradiation received by a cell during the day and the cell temperature (T_{cell}). Finally, we incorporate the proposed empirical correlation into the EY model and thus obtain an excellent agreement between simulation and measurements during the whole day. Using the upgraded EY model, we predict the annual energy yield losses associated with the studied metastability effect in both single junction and tandem devices and discuss the implications of device orientation and geographical location.

2. Outdoor Data

This work is based on the outdoor performance data of p-i-n perovskite solar cells in a single-junction (SJ) architecture as well as in a PK-Si tandem architecture, all operating at maximum power point (MPP). The single-junction devices, with a perovskite bandgap of E_G = 1.52 eV, were structured as follows: ITO/ MeO-2PACz / formamidinium lead iodide ($FAPbI_3$) perovskite/ LiF/ C60/ SnO_2/ Cu and exhibited an average PCE of 16.6% after encapsulation. Tandems were manufactured using a silicon heterojunction bottom cell and a p-i-n, wide bandgap (E_G = 1.68 eV) triple-cation perovskite ($Cs_{0.05}(FA_{0.77}MA_{0.23})_{0.95}Pb(I_{0.77}Br_{0.23})_3$) top cell with a similar architecture as described in.[32] After encapsulation, an average PCE of 24.2% was measured. The selected device structures are representative of the high-efficiency SJ and tandem devices, with the latter requiring a higher bandgap perovskite that is achieved through compositional engineering.

All of the studied solar cells were small-size with an active area of 0.16 cm^2 (for single junction) and 1 cm^2 (for tandems). All devices were encapsulated based on the glass-glass technique that uses butyl rubber as an edge sealant and polyolefin (POE) film as an encapsulant[10] (refer to the supporting information for details). One $FAPbI_3$ device in the batch had no POE encapsulant, only edge sealant – this did not affect its daily behavior or long-term performance degradation. Encapsulated devices were mounted on a fixed optimal tilted (35°) stand facing south and connected to a maximum power point tracking system.[33] The long-term performance data was recorded in parallel with weather conditions, such as the absolute and spectrally-resolved irradiance in the plane of array and cell temperature (T_{cell}).

We performed the long-term outdoor measurements on the HZB rooftop test field located in Berlin, Germany (**Figure 1a**)) over the period of October 2020 – June 2023 (33 months or 972 days) for four SJ devices and December 2021 – November 2022 (11 months or 322 days) for four tandem devices. In both cases, these are among the largest datasets available in the literature at the moment. In Figure 1d) the data is represented as averaged midday outdoor PCE ($PCE_{outdoor}$) values for the devices exposed to the outdoor conditions in Berlin. The $PCE_{outdoor}$ was calculated based on device power output and absolute irradiance in the plane of array with no temperature or spectral mismatch correction applied in the calculations. The encapsulated SJ devices show good outdoor stability, retaining about 65% of the initial $PCE_{outdoor}$ after 2.5 years of outdoor exposure. Nevertheless, seasonal changes in device performance are evident, with increased performance during the summer months and a drop in performance during the winter months.[34] Summer decline would have been expected due to no temperature compensation in $PCE_{outdoor}$ calculations, however, the trend is the opposite. Additionally, by comparing summer-to-summer peak $PCE_{outdoor}$ values, a relatively slow long-term degradation trend can be noticed, showing promise for the long-term stable behavior of perovskite solar cells. The degradation between the winter-to-winter minimum is larger in the first year, with little change from the second to third winter. Tandem devices show an initial increase in

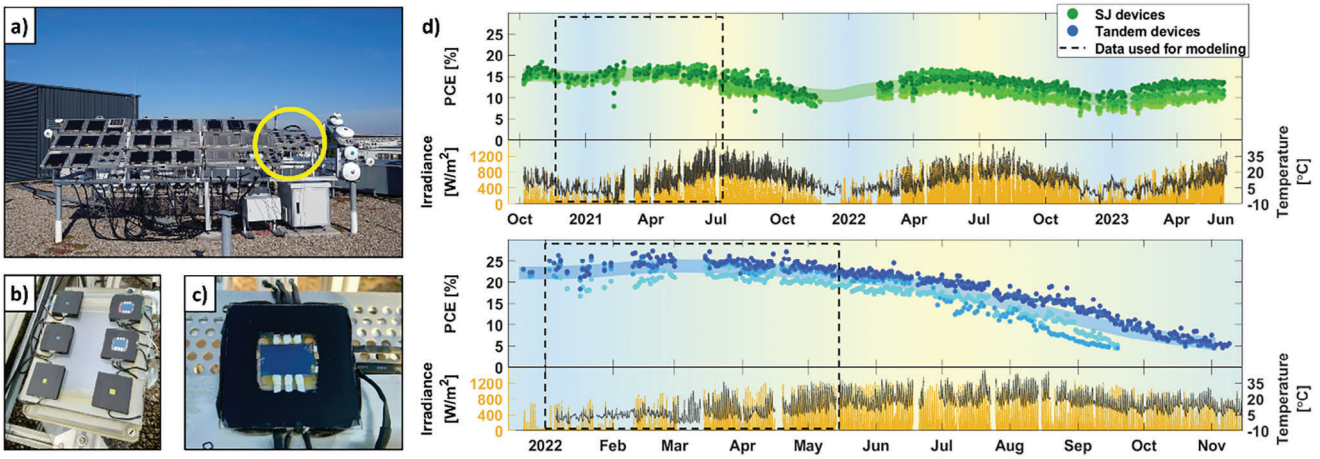

Figure 1. Experimental outdoor data. a) Rooftop test field in Berlin; area with lab-scale perovskite devices marked with a yellow circle. Example of encapsulated tandem and single-junction devices mounted on the test fields in b) Ljubljana and c) Berlin. d) Long-term outdoor data for SJ perovskite (green) and PK-Si tandem (blue) devices. Dots represent average midday PCE values of the devices, calculated for irradiances higher than 150 W m^{-2} (the line serves as guide to the eye). Global irradiance measured in the plane of array (orange) and the temperature of a device (black) are also shown. Black dashed rectangles in d) mark the recording period that was used for EY model validation. Part of the dataset in Figure 1d) (SJ devices; top panel) was extended and adapted from our previously reported data.[34]

$PCE_{outdoor}$ from spring to summer, which is likely due to seasonal changes in weather, as observed in the case of single-junction devices. However, their performance starts to noticeably degrade throughout the summer and autumn. High operating temperatures, current mismatch changes, potential encapsulation-related issues, or simply higher doses of irradiation may be among the causes of the observed acceleration in device degradation. Even though the long-term device degradation is noticeable over a longer period, it is difficult to disentangle the seasonality effects from the actual loss of device performance just by using the experimental outdoor data. Only by comparing outdoor data with the EY model results, we can clearly detect and quantify the long-term degradation. Although quantifiable, the exact origins of the device degradation are beyond the scope of this paper. Here we focus on the relatively stable parts of the datasets (marked with black dashed rectangles in Figure 1d)) to validate and train our EY model that includes also short-term diurnal metastable effects.

In addition to variations in performance due to seasonality and long-term degradation, both types of devices also exhibit daily reversible changes – so-called metastability, which is the main focus of this paper. In studied solar cells, this phenomenon is most noticeable in the V_{MPP} values throughout the day. **Figure 2a)** shows V_{MPP} and irradiance data for the $FAPbI_3$ SJ device over the course of four consecutive relatively sunny days, whereas Figure 2b) demonstrates the V_{MPP} at different times of the day (indicated by color) as a function of incident irradiance. We observe an increasing trend in V_{MPP} throughout almost the whole day that is way steeper than the logarithmic voltage increase expected solely due to higher irradiance. The comparison of morning and evening V_{MPP} values at the same irradiance shows that the evening values are consistently higher than the morning ones, and also that the same V_{MPP} values are repeatedly reached when the cell becomes fully light-soaked. Therefore, the increase of V_{MPP} (and, consequently, $PCE_{outdoor}$) in the morning hours should be regarded as

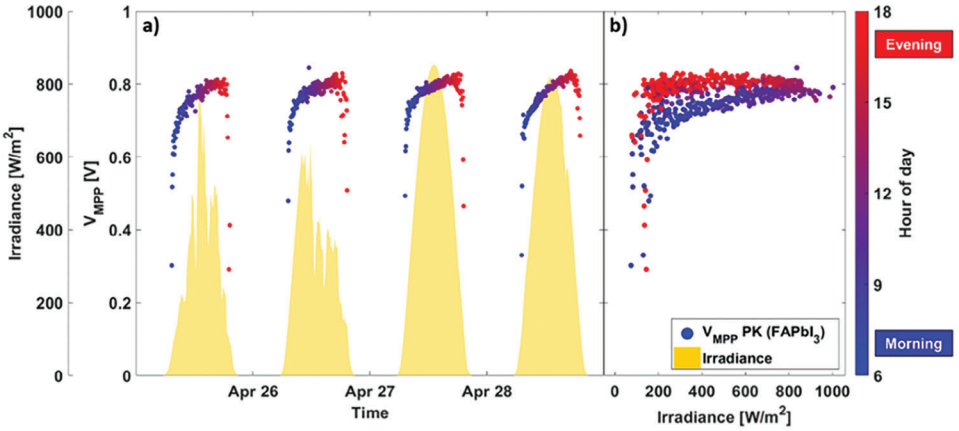

Figure 2. LSE in outdoor data for $FAPbI_3$-based SJ perovskite solar cells. The maximum power point voltage (color-coded for the hour of the day) during several days of observation as a function of a) time and b) irradiance. The irradiance during the corresponding days is shown in yellow.

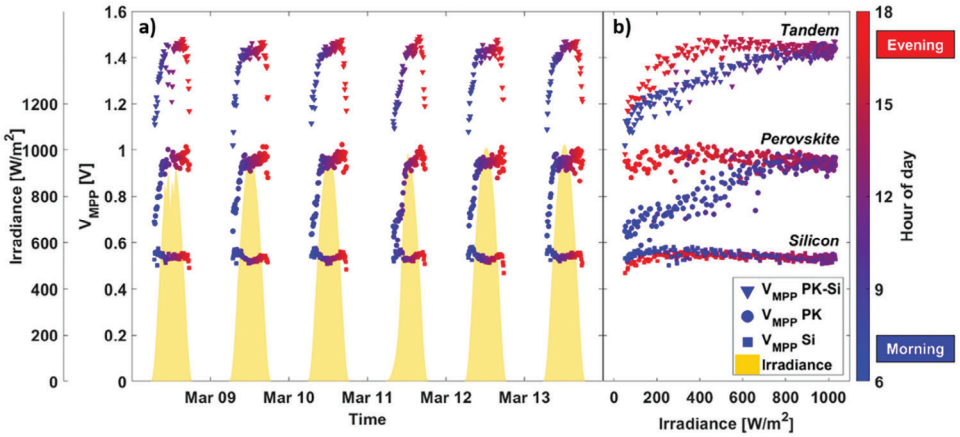

Figure 3. LSE in outdoor data for PK-Si tandem device as well as for the reference single-junction silicon and perovskite cells with the same structure as the tandem sub-cells. The maximum power point voltage (color-coded for the hour of the day) during several days of observation as a function of a) time and b) irradiance. The irradiance during the corresponding days is shown in yellow.

a recovery rather than an improvement – light-soaking during the day gradually eliminates the negative effects of nighttime degradation and, if weather conditions allow, returns the cell's performance to its initial (peak) state.

To analyze the metastability behavior in the individual sub-cells of a tandem device, an additional set of outdoor measurements was conducted on a rooftop monitoring site of LPVO in Ljubljana (Slovenia). The outdoor measurements were carried out in parallel for the PK-Si tandem device as well as for the single-junction high bandgap perovskite and silicon devices that have the exact same structure as the tandem top and bottom sub-cell. **Figure** 3a) shows the V_{MPP} data for all three devices over the course of several consecutive sunny days at the beginning of the device operation and Figure 3b) represents the V_{MPP} values at different times of the day (indicated by color) as a function of incident irradiance.

For the SJ Si solar cell, the V_{MPP} is relatively unchanged throughout the day, except for a marginal decrease towards midday due to higher operating temperatures. Conversely, the V_{MPP} values of the high bandgap perovskite SJ solar cell are affected by the LSE in a qualitatively similar way as shown for the low bandgap SJ $FAPbI_3$ perovskite device in Figure 2, despite having a different perovskite absorber. Such metastable behavior is then translated into the operation of the PK-Si tandem device, leading to light-soaking dynamics that are similar to those of the perovskite SJ devices. We can observe a good correlation between the sum of the voltages of PK and Si single-junction devices and the measured V_{MPP} of the PK-Si tandem device. In the evening hours, the decrease of V_{MPP} occurs earlier for the PK-Si tandem device than for the other two device types. We attribute this behavior to the lower value of the shunt resistance (R_{SHUNT}) of that particular tandem device compared to the R_{SHUNT} of the SJ perovskite or Si solar cell.

Overall, our outdoor measurements reveal that perovskite-based devices lose a considerable amount of energy in the mornings due to the LSE. The exact extent of losses, however, remains unknown, since experimental data alone is not sufficient to separate the light-soaking effect from the effects of constantly changing environmental parameters that also affect the energy yield of PV devices. For this, the energy yield model that emulates the device performance in real-world conditions plays a key role.

3. Modelling

Numerical modelling in our work was employed for two specific purposes. Firstly, to extract and quantify the losses associated with the light-soaking effect in any particular PK-based solar cell technology directly from outdoor measurements performed under realistic operating conditions. And secondly, to implement the LSE mechanism into the energy yield modelling framework to predict, analyze and compare long-term LSE losses in different operating conditions.

We used an in-house developed EY algorithm[29] that is based on three key modelling approaches (optical, thermal, and electrical). As the input data, we applied realistic optical constants of the materials, layer thicknesses, and interface textures, as well as measured device operating temperature (T_{cell}) and meteorological data (spectrally resolved global tilted irradiance (GTI) and direct normal irradiance (DNI), etc.) acquired on the HZB outdoor PV monitoring site. The electrical behavior of the device was modelled based on an extensive set of *J-V* characteristics measured on a fresh device under well-defined indoor conditions (irradiance/temperature), following the methodology outlined in.[29] The measured, fresh device was completely light-soaked prior to each *J-V* measurement to factor out any metastable behavior. The optical part of the model was validated for the selected PK-Si tandem devices by comparing the modelled and measured external quantum efficiency (EQE) and short-circuit current densities (J_{sc}) of the device's sub-cells under STC conditions (Figure S4, Supporting Information).

Figure 4 shows the measured and simulated a) voltage (V_{MPP}), b) short-circuit current density (J_{MPP}), and c) power (P_{MPP}) values at MPP of the investigated PK-Si tandem device over the course of six selected days at the beginning of the device operation along with d) the acquired incident irradiance (GTI) and device temperature (T_{cell}). While the simulated (red curve) and measured (blue

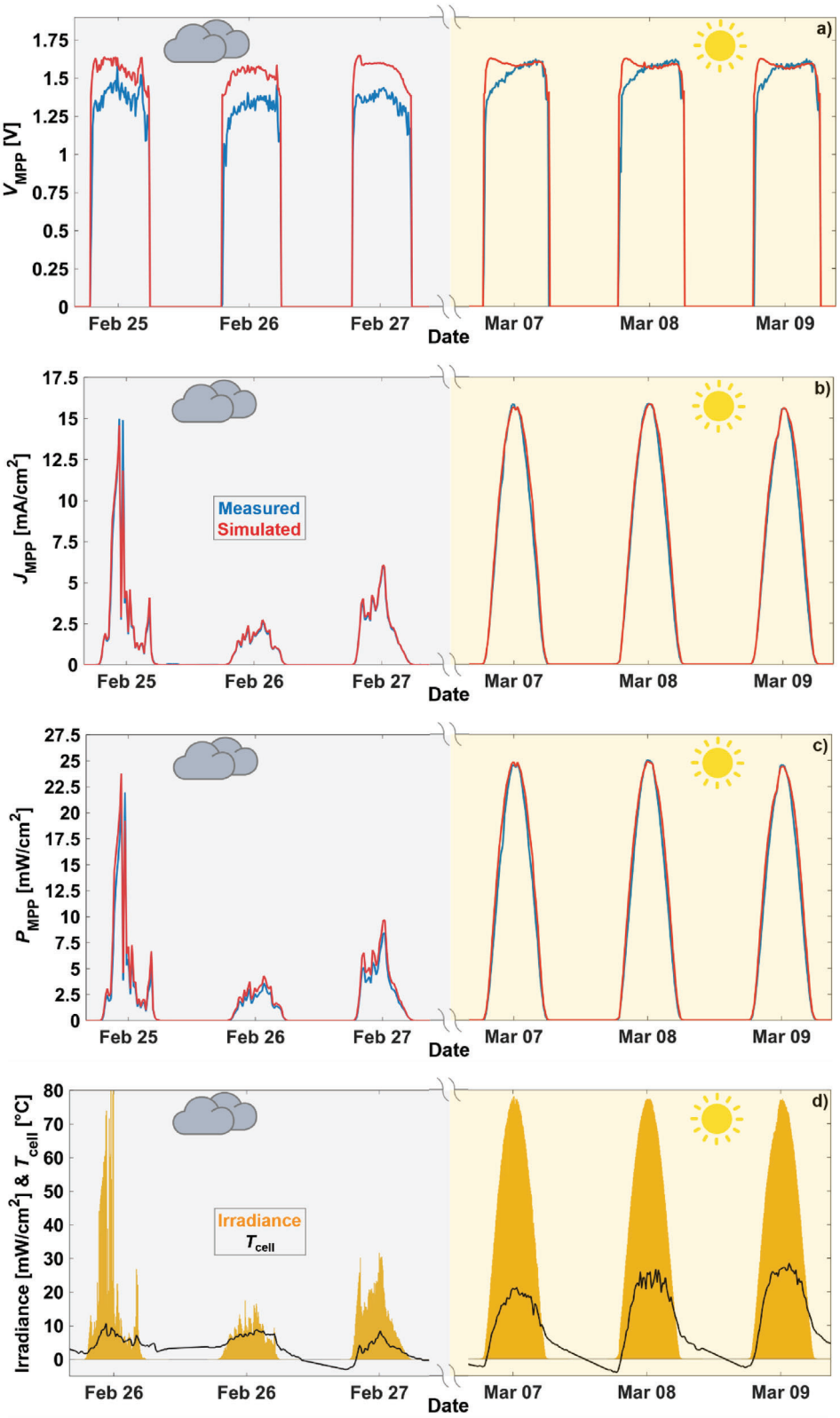

Figure 4. Measured (blue curve) and simulated (red curve) a) V_{MPP}, b) J_{MPP}, and c) P_{MPP} values of the PK-Si tandem device over the course of three consecutive cloudy and three consecutive sunny days. d) Measured total incident irradiance (yellow area) and device operating temperature (black curve) for the six selected days.

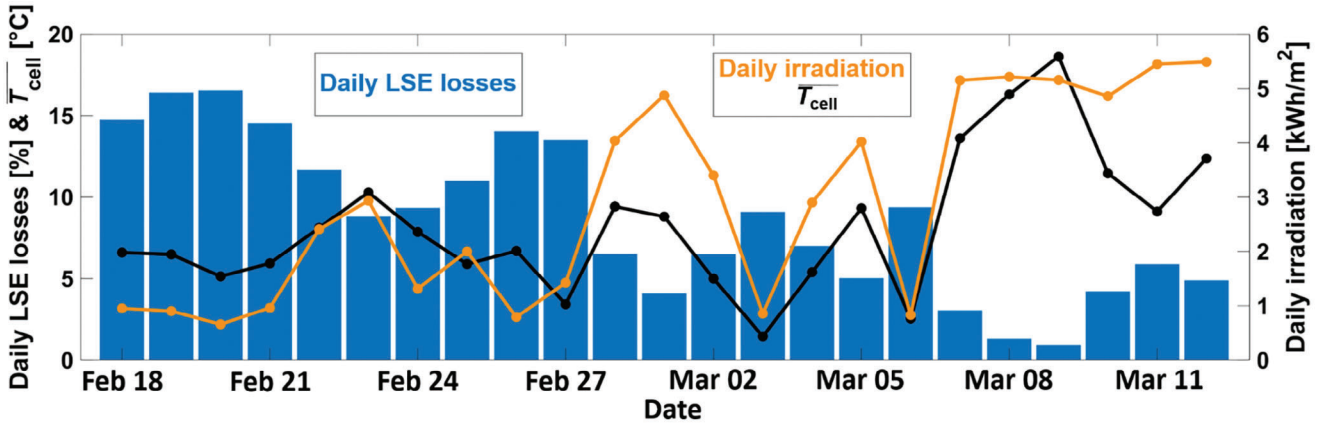

Figure 5. Daily energy generation losses of the tandem device attributed to the LSE effect over the course of three consecutive weeks. Also plotted are the daily irradiation (orange curve) and the daily average of device temperature (black curve).

curve) J_{MPP} values in Figure 4b) show a good agreement, there is a notable discrepancy between the simulated and measured V_{MPP} and, consequently, also P_{MPP} values (although less visible due to a larger span of the P_{MPP} vertical axis). On cloudy days, the measured V_{MPP} values are lower than the simulated ones throughout the whole day. On sunny days, however, the measured values deviate from the simulated ones only in the morning hours but match closely in the afternoon. We attribute this V_{MPP} difference to the LSE, since during the second half of each sunny day when the device is fully light-soaked, the measurements overlap with the simulations. This good agreement between the results obtained for fully light-soaked cells indicates the validity of our EY modelling approach, which allows us to calculate, at any given operating conditions, the predicted (ideal) power generation of the device without any degradation or metastability effects.

3.1. LSE Extraction and Quantification

Ideal EY simulation results in comparison to actual outdoor measurements can be used to extract and quantify the extent of the LSE losses during the device operation. The results in Figure 4c) show that energy losses are substantial in low irradiance conditions, amounting to around 12% for the three cloudy days shown. On sunny days, however, when the device is fully light-soaked in the afternoon hours, the losses are significantly lower, totaling approximately 2% over the selected three days.

The same methodology can be used also for longer time periods of the outdoor operation. **Figure 5** shows the daily losses attributed to the LSE over the course of three weeks (before any significant irreversible degradation of the device could be observed). The daily sum of the incident irradiance (daily irradiation) and the daily average of device temperature ($\overline{T_{cell}}$) are also plotted. The results show that over the course of these three weeks, the LSE losses reduce the total achievable generated energy obtained with the EY model by 6%. Again, it can be observed that the losses vary from day to day, but are closely correlated with the device operating conditions, with larger LSE losses observed on days with lower daily irradiation and lower device temperature.

3.2. LSE Modelling

To predict the amount of LSE losses in different environmental and installation cases, the LSE mechanism needs to be

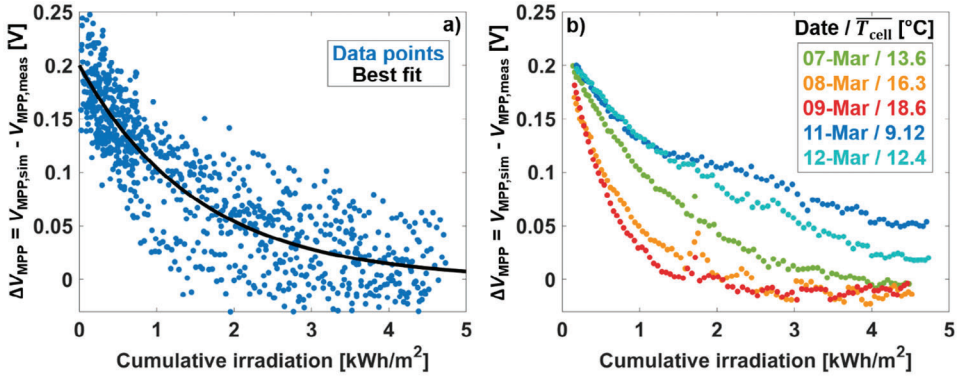

Figure 6. a) The difference between simulated and measured V_{MPP} results (ΔV_{MPP}) of the PK-Si tandem cell as a function of the cumulative irradiation (H_{cum}). With the increasing cumulative irradiation H_{cum}, the difference between the simulated and measured V_{MPP} approaches 0 V. b) A smaller set of ΔV_{MPP} results for five selected days (March 7th – 9th, 11th and 12th). The average daily operating temperature of the tandem device ($\overline{T_{cell}}$) is also stated.

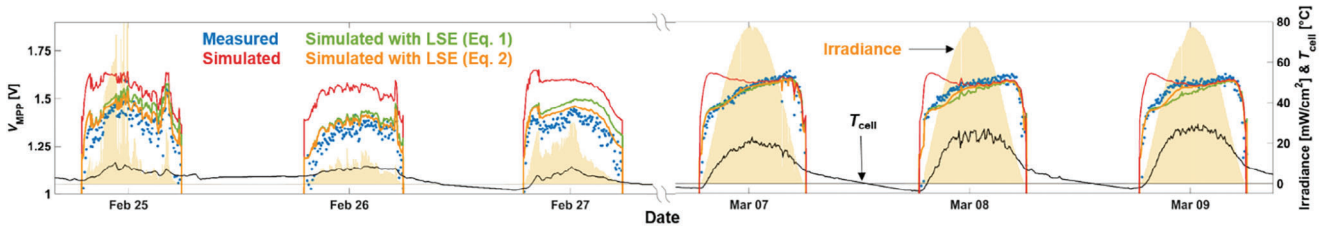

Figure 7. Measured (blue dots) and ideal simulated (red curve) V_{MPP} values of the PK-Si tandem device over the course of six days in March 2022. For better visualization, the V_{MPP} data are presented from 1 V onwards. Also shown are the modelled V_{MPP} values that include light-soaking effect obtained by using Equation (1) (green curve; $A = 0.2$ V, $\tau = 1.5354$ kWh m^{-2}) and Equation (2) (orange curve; $A = 0.2$ V, $B = 6.99{*}10^7$ (kWh m^{-2})-1, $E_a = 0.4616$ eV) as well as measured device operating temperature and incident irradiance.

implemented into the EY modelling algorithm. We selected several days in March 2022 and calculated the difference between the simulated and measured V_{MPP} ($\Delta V_{MPP} = V_{MPP,sim} - V_{MPP,meas}$). For each data point, we also calculated the cumulative irradiation $H_{cum}(t)$ that was intercepted by the tandem device from sunrise up to the given time of day: $H_{cum}(t) = \sum_{sunrise}^{t} \left(\int_{300\ nm}^{1200\ nm} GTI(\lambda)\, d\lambda \right) \cdot \Delta t$, where λ is the wavelength of the incoming light, t represents the data point's time of day and Δt denotes the measurement resolution. The relation between ΔV_{MPP} and H_{cum} is presented in **Figure 6a**). As expected, with increasing cumulative irradiation H_{cum} the cell becomes more and more light-soaked, and the difference between the simulated and measured V_{MPP} approaches 0 V.

For the initial approximation, the correlation between the LSE-induced voltage deficit ΔV_{MPP} and cumulative irradiation can be modelled by fitting the data points presented in Figure 6a) with an exponential decay function (black line):

$$\Delta V_{MPP} = A e^{-\frac{H_{cum}}{\tau}} \quad (1)$$

The comparison between the measured (blue dots) V_{MPP} and simulated (green curve) values with LSE is presented in **Figure 7** together with simulated V_{MPP} values without LSE (red curve) and device operating conditions. While an improvement in agreement is achieved, there are nevertheless significant discrepancies between the results in certain conditions, presumably stemming from the scattered points around the fit in Figure 6a).

It was shown in previous reports,[17,23] that under STC conditions, the LSE is affected not only by irradiation but also by the device temperature. Indeed, this can already be observed in Figure 4a) for sunny days, where measured results begin to agree with the simulations at different times each day, despite almost identical irradiance conditions. We attribute this to the difference in daily T_{cell} profiles. We selected and replotted a smaller set of previously presented ΔV_{MPP} results that represents five days with very similar irradiance conditions, yet notably different LSE dynamics, as clearly shown in Figure 6b). It can be noticed that ΔV_{MPP} declines faster at higher average daily operating temperature ($\overline{T_{cell}}$; the calculated values are indicated in Figure 6b)), showing that the LSE is accelerated by the temperature. Following this observation, we upgraded Equation (1) so that the rate constant τ varies with temperature according to the Arrhenius equation,[35] as given in Equation (2), where k_B represents the Boltzmann constant:

$$\Delta V_{MPP} = A e^{-\frac{H_{cum}}{\tau}};\ \frac{1}{\tau} = B e^{-\frac{E_a}{k_B T_{cell}}} \quad (2)$$

Once again, constants A, B, and E_a were selected to best fit the data points in Figure 6b), and the model was implemented in our EY algorithm. The simulated V_{MPP} results obtained by using the upgraded model are presented in Figure 7 (orange curve) together with previous results. A much better agreement with the experimental values can now be observed in all cases, demonstrating the importance of including T_{cell} in the LSE model. The remaining small discrepancy between the model and measurements can be attributed to other factors, for example, the spread of measured MPP values due to changing environmental conditions, or the impact of the history of device conditions longer than just one day. However, we did not investigate these factors

Table 1. Summary of numerical results for both solar cells and for each of the four geographical locations from distinct KGPV zones.[36] Tabulated are the yearly EY values with and without LSE as well as the relative energy losses associated with the effect.

Solar cell	PK-Si tandem						PK single-junction		
Orientation	optimal			vertical			optimal		
Location	EY without LSE [kWh m^{-2}]	EY with LSE [kWh m^{-2}]	LSE losses [%]	EY without LSE [kWh m^{-2}]	EY with LSE [kWh m^{-2}]	LSE losses [%]	EY without LSE [kWh m^{-2}]	EY with LSE [kWh m^{-2}]	LSE losses [%]
Panama	463.2	457.1	1.3	161.6	155.3	3.9	313.4	307.0	2.0
Denver	524.4	511.6	2.4	317.2	305.2	3.8	341.5	328.4	3.8
Atlanta	477.8	468.7	1.9	252.1	243.5	3.4	319.3	309.7	3.0
Columbus	420.0	406.9	3.1	239.8	228.1	4.9	280.8	266.9	4.9

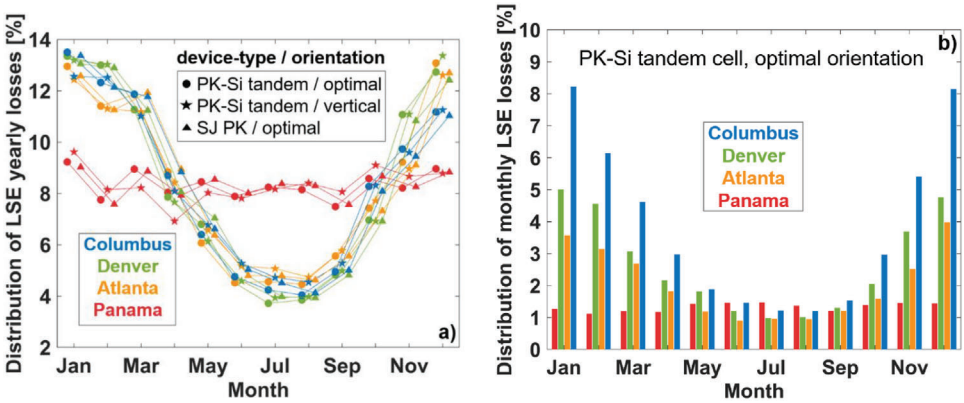

Figure 8. a) The relative distribution of the calculated location-specific yearly LSE losses over different months of the year for the PK-Si tandem solar cell in optimal and vertical open-rack configuration as well as for the PK single-junction solar cell in optimal orientation. b) The absolute distribution of the location-specific monthly LSE losses for the PK-Si tandem solar cell.

further since we wanted to keep the model relatively simple, and especially since the discrepancy between the simulated and measured generated energy is already less than 0.25% for the case of the selected six days and less than 0.8% for the case of the extended period of three consecutive weeks (Feb 18th – Mar 12th). A similarly good agreement for SJ $FAPbI_3$ PK solar cell is shown in (Figure S5, Supporting Information).

It should be noted that the presented analysis was performed for a time period where the devices (both tandem and SJ) did not show any irreversible degradation. However, under prolonged outdoor operation, solar cells are subjected to different degradation mechanisms which also affect the LSE dynamics and thus the parameter values used in Equation (2). In this contribution, we focused only on the metastability detection, quantification, and methodology of its inclusion into the energy yield model. The irreversible degradation and its influence on different aspects of the device outdoor operation, including the light-soaking effect, go beyond the scope of this contribution and will be regarded in future work.

4. Analysis of Long-Term LSE Losses

Finally, the comprehensive EY modelling algorithm upgraded with LSE metastability was used to study the long-term energy losses in different environmental conditions (geographical locations). The LSE dynamics was modelled according to Equation (2), where it was assumed that the parameters of the decay functions do not change in time. No other degradation mechanisms beyond LSE were taken into consideration.

We analyzed the following two PV devices, a) the complete PK-Si tandem solar cell investigated in the previous section, and b) a high bandgap triple-cation single-junction PK solar cell that represents the top sub-cell of the tandem device. Four North America-based geographical locations were selected from different climate zones according to the Köppen-Geiger (KGPV) classification[36] (zone designations are provided in parentheses): Panama (AH), Denver (CH), Atlanta (DH), and Columbus (DM). The selected zones have very different environmental conditions and cover a large area of the USA as well as Europe. All relevant meteorological data (spectrally-resolved GTI and DNI, ambient temperature, wind speed) were obtained from the National Solar Radiation Database[37] for each installation of the devices. It should be noted that Berlin, from where the outdoor measurements presented in previous sections were acquired, belongs to the DL KGPV climate zone. The latter has similar environmental conditions to the DM zone, however it has even lower yearly insolation and ambient temperatures.

The extent of the LSE losses for each of the two devices and for each of the selected locations was first evaluated on a yearly basis. Both devices were studied in optimal location-specific open-rack orientation, whereas for the case of the tandem cell also vertical configuration was considered. The results are summarized in **Table 1**. For the case of optimal orientation, it can be observed that minimal LSE losses are achieved in Panama for both devices (1.3% for the tandem and 2.0% for the single-junction device). This was expected since Panama represents a location with relatively high insolation and ambient temperature throughout the whole year. Both influence the LSE dynamics in a favorable way from the device performance viewpoint. In contrast, the device installed in Columbus would experience nearly 3 times higher yearly LSE losses (3.1% and 4.9%, respectively) due to the less favorable conditions;, i.e., less sun and lower temperature. In all cases, we notice that the LSE losses are much lower in the tandem device, although both cells experience the same LSE dynamics. The reason for this is in the bottom Si sub-cell, which in a PK-Si tandem device contributes one-third of the total output energy and does not exhibit LSE. The results corresponding to the vertical configuration show that even without considering the LSE, the generated energy of the tandem cell is reduced by more than 40% in all selected locations due to a decrease in incoming solar energy. The yearly LSE losses are increased accordingly, which is especially notable in the case of Panama (3 times higher) since the difference between the optimal (13°) and the vertical (90°) inclination of the device is the largest there. Denver has the smallest difference between the inclination angles and thus the smallest increase in yearly LSE losses.

Due to the pronounced influence of the LSE dynamics on the environmental conditions, it is expected that the seasonal variations also affect how LSE losses are distributed over the year. To confirm and further investigate this phenomenon, we calculated

the relative distribution of yearly LSE losses over the months. The results are presented in **Figure** 8a) for the PK-Si tandem solar cell in optimal and vertical open-rack configuration as well as for the SJ PK solar cell in optimal orientation (refer to Figure S6, Supporting Information for absolute distribution of yearly LSE losses over the months). In all three device-type/installation cases, we get a very similar relative distribution of losses regardless of the geographical location. Moreover, the practically identical relative distribution also applies to the devices installed in seasonal conditioned climates, represented by Denver, Atlanta, and Columbus. The results for these three locations indicate that during winter months, the contribution to total yearly losses is ≈ three times higher compared to the summer months due to significantly lower insolation, which is directly related to the combination of total irradiance and ambient temperature. By contrast, since Panama is located near the equator, the seasonal variations in environmental conditions are very small, which results in a near-uniform relative distribution of LSE losses.

Finally, the extent of LSE losses can also be evaluated on a monthly basis, which can be important for season-based investigation and optimization of device operation. For this purpose, we calculated the ratio between the energy lost due to the LSE and the ideal energy generated within each month, as plotted in Figure 8b) for the PK-Si tandem device. For each selected geographical location except Panama, it is evident that in winter the device can lose a notable amount of the potentially generated energy due to LSE. This is especially evident for Columbus (Lat. 40° N), which is a geographical location with a distinctly seasonal conditioned climate. With monthly LSE losses of over 8% in winter, they are more than seven times larger than those in summer.

5. Conclusion

Reliable outdoor operation of perovskite-based solar cell with improved long-term stability is crucial for the industrialization of the technology; however, reports of thorough outdoor testing and in-depth analysis of the results are still lacking. In this work, we demonstrated long-term (several months up to 2.5 years) outdoor monitoring data of several single-junction perovskite and perovskite-silicon tandem devices under MPP conditions. Both types exhibited promising stability, especially SJ devices with 65% of the initial $PCE_{outdoor}$ retained after 2.5 years of testing. In both types of devices, however, a peculiar behavior can be observed in the morning hours, particularly on cloudy days, where the solar cell performance is at first lower than expected, but then gradually recovers to the initial STC performance during the day under sunlight. We attribute this to the metastable process of nighttime degradation and the subsequent light-induced recovery of the perovskite material, which is known as the light-soaking effect, LSE.

To extract the parameters of LSE from outdoor measurements, we applied a state-of-the-art EY model calibrated with the specifics of fresh, fully light-soaked SJ and tandem solar cells that served as the LSE-free reference to which the measured data are compared. This enabled us to quantify the energy production losses associated with the metastability in a PK-Si tandem device operating in real-world conditions in Berlin over the course of three consecutive weeks, which amount to a total of 6%. Additional analysis of the results revealed that the voltage drop and the rate of recovery associated with the LSE depends on the daily cumulative irradiation as well as the operating temperature, and all three parameters can be empirically interconnected using an Arrhenius equation.

In the final part of our study, we incorporated the empirical relation of the LSE dynamics into our EY model, which allowed us, for the first time, to model long-term real-world device operation by taking the effects of the studied metastability fully into account. Using the upgraded EY model, we analyzed the energy harvesting losses associated with the LSE over the course of one typical meteorological year, for different types of devices operating in different geographical locations and in different orientation/installation cases. Results showed that, depending on the location/climate, yearly LSE losses can amount to up to 3% in an optimally oriented PK-Si tandem solar cell, and monthly even up to 8%. This not only highlights the notable impact of LSE and the necessity for its accurate evaluation, but also reveals that in geographic regions with pronounced seasonal variations, wintertime performance of perovskite-based solar cells can be significantly lower than summertime performance – contrary to conventional PV technologies. With the presented methodology of combined outdoor measurement and EY modelling, both can be easily evaluated, leading to faster development of perovskite solar cells on their road towards commercialization.

Supporting Information

Supporting Information is available from the Wiley Online Library or from the author.

Acknowledgements

M. R. and Š. T contributed equally to this work. The authors thank the Helmholtz Association for funding the project TAPAS (Tandem Perovskite And Silicon solar cells—Advanced optoelectrical characterization, modelling and stability) within the EU partnering program. C.U. and R.S. acknowledge the support by the Helmholtz Association, Germany under the program "Energy System Design". The authors acknowledge the financial support from the Slovenian Research Agency (program P2-0415 and project J2-1727). Š.T. also thanks the Slovenian Research Agency for her Ph.D. funding.

Open access funding enabled and organized by Projekt DEAL.

Conflict of Interest

The authors declare no conflict of interest.

Data Availability Statement

The data that support the findings of this study are available from the corresponding author upon reasonable request.

Keywords

energy yield modelling, light-soaking effect, outdoor monitoring, perovskite-based solar cells, realistic operating conditions

Received: December 22, 2023
Revised: April 19, 2024
Published online: May 9, 2024

[1] "Best Research-Cell Efficiency Chart." [Online]. https://www.nrel.gov/pv/cell-efficiency.html, July **2022**.
[2] M. A. Green, E. D. Dunlop, G. Siefer, M. Yoshita, N. Kopidakis, K. Bothe, X. Hao, *Prog. Photovolt. Res. Appl.* **2023**, *31*, 3.
[3] X. Zhao, T. Liu, Q. C. Burlingame, T. Liu, R. Holley, G. Cheng, N. Yao, F. Gao, Y.-L. Loo, *Science* **2022**, *377*, 307.
[4] Q. Jiang, R. Tirawat, R. A. Kerner, E. A. Gaulding, Y. Xian, X. Wang, J. M. Newkirk, Y. Yan, J. J. Berry, K. Zhu, *Nature* **2023**, *623*, 313.
[5] M. Jost, B. Lipovsek, B. Glazar, A. Al-Ashouri, K. Brecl, G. Matic, A. Magomedov, V. Getautis, M. Topic, S. Albrecht, *Adv. Energy Mater.* **2020**, *10*, 2000454.
[6] Q. Emery, M. Remec, G. Paramasivam, S. Janke, J. Dagar, C. Ulbrich, R. Schlatmann, B. Stannowski, E. Unger, M. Khenkin, *ACS Appl. Mater. Interfaces* **2022**, *14*, 5159.
[7] J. Li, J. Dagar, O. Shargaieva, O. Maus, M. Remec, Q. Emery, M. Khenkin, C. Ulbrich, F. Akhundova, J. A. Márquez, T. Unold, M. Fenske, C. Schultz, B. Stegemann, A. Al-Ashouri, S. Albrecht, A. T. Esteves, L. Korte, H. Köbler, A. Abate, D. M. Többens, I. Zizak, E. J. W. List-Kratochvil, R. Schlatmann, E. Unge, *Adv. Energy Mater.* **2023**, *13*, 2203898.
[8] M. Babics, M. De Bastiani, E. Ugur, L. Xu, H. Bristow, F. Toniolo, W. Raja, A. S. Subbiah, J. Liu, L. V. Torres Merino, E. Aydin, S. Sarwade, T. G. Allen, A. Razzaq, N. Wehbe, M. F. Salvador, S. De Wolf, *Cell Rep. Phys. Sci.* **2023**, *4*, 101280.
[9] M. De Bastiani, E. Van Kerschaver, Q. Jeangros, A. Ur Rehman, E. Aydin, F. H. Isikgor, A. J. Mirabelli, M. Babics, J. Liu, S. Zhumagali, E. Ugur, G. T. Harrison, T. G. Allen, B. Chen, Y.i Hou, S. Shikin, E. H. Sargent, C. Ballif, M. Salvador, S. De Wolf, *ACS Energy Lett.* **2021**, *6*, 2944.
[10] M. V. Khenkin, A. K. M., I. Visoly-Fisher, Y. Galagan, F. Di Giacomo, B. R. Patil, G. Sherafatipour, V. Turkovic, H.-G. Rubahn, M. Madsen, T. Merckx, G. Uytterhoeven, J. P. A. Bastos, T. Aernouts, F. Brunetti, M. Lira-Cantu, E. A. Katz, *Energy Environ. Sci.* **2018**, *11*, 739.
[11] C. Zhao, B. Chen, X. Qiao, L. Luan, K. Lu, B. Hu, *Adv. Energy Mater.* **2015**, *5*, 1500279.
[12] M. V. Khenkin, A. K. M., I. Visoly-Fisher, S. Kolusheva, Y. Galagan, F. Di Giacomo, O. Vukovic, B. R. Patil, G. Sherafatipour, V. Turkovic, H. G. Rubahn, M. Madsen, A. V. Mazanik, E. A. Katz, *ACS Appl. Energy Mater.* **2018**, *1*, 799.
[13] L. Jiang, J. Lu, S. R. Raga, J. Sun, X. Lin, W. Huang, F. Huang, U. Bach, Y.i-B. Cheng, *Nano Energy* **2019**, *58*, 687.
[14] L. Lin, L. Yang, G. Du, X. Li, Y.-N. Li, J. Deng, K. Wei, J. Zhang, *ACS Appl. Energy Mater.* **2023**, *6*, 10303.
[15] B. Roose, *RSC Adv.* **2021**, *11*, 12095.
[16] J. Herterich, M. Unmüssig, G. Loukeris, M. Kohlstädt, U. Würfel, *Energy Technol.* **2021**, *9*, 2001104.
[17] B. Li, M. Lin, C. Kan, P. Hang, Y. Yao, Z. Hu, Y. Wang, Y. Zhang, W. Zhong, D. Yang, X. Yu, *Sol. RRL* **2022**, *6*, 2200050.
[18] J. Peng, Y. Sun, Y. Chen, Y. Yao, Z. Liang, *ACS Energy Lett.* **2016**, *1*, 1000.
[19] B. Cai, X. Yang, Z.e Yu, Y. Liang, Y.u Shan, A. Hagfeldt, L. Sun, *J. Power Sources* **2020**, *472*, 228506.
[20] E. Mosconi, D. Meggiolaro, H. J. Snaith, S. D. Stranks, F. D. Angelis, *Energy Environ. Sci.* **2016**, *9*, 3180.
[21] J. Wang, X. Duan, W. J. Yin, *J. Phys. Chem. Lett.* **2021**, *12*, 9328.
[22] H. Tsai, R. Asadpour, J. C. Blancon, C. C. Stoumpos, O. Durand, J. W. Strzalka, B.o Chen, R. Verduzco, P. M. Ajayan, S. Tretiak, J. Even, M. A. Alam, M. G. Kanatzidis, W. Nie, A. D. Mohite, *Science* **2018**, *360*, 67.
[23] X. Wu, J. Ma, M. Qin, X. Guo, Y. Li, Z. Qin, J. Xu, X. Lu, *Adv. Funct. Mater.* **2021**, *31*, 2101287.
[24] X. Zhang, S. H. Wei, *Phys. Rev. Lett.* **2022**, *128*, 136401.
[25] T. J. Silverman, M. G. Deceglie, I. R. Repins, T. Zhu, Z. Song, M. J. Heben, Y. Yan, C. Fei, J. Huang, L. T. Schelhas, *IEEE J. Photovolt.* **2023**, *13*, 740.
[26] J. Lehr, M. Langenhorst, R. Schmager, S. Kirner, U. Lemmer, B. S. Richards, C. Case, U. W. Paetzold, *Sustain. Energy Fuels* **2018**, *2*, 2754.
[27] R. Schmager, M. Langenhorst, J. Lehr, U. Lemmer, B. S. Richards, U. W. Paetzold, *Opt. Express* **2019**, *27*, A507.
[28] P. Tillmann, K. Jäger, A. Karsenti, L. Kreinin, C. Becker, *Sol. RRL* **2022**, *6*, 2200079.
[29] Š. Tomšič, M. Jošt, K. Brecl, M. Topič, B. Lipovšek, *Adv. Theory Simul.* **2023**, *6*, 2200931.
[30] M. T. Hörantner, H. J. Snaith, *Energy Environ. Sci.* **2017**, *9*, 1983.
[31] F. Gota, R. Schmager, A. Farag, U. W. Paetzold, *Opt. Express* **2022**, *30*, 14172.
[32] A. Al-Ashouri, E. Köhnen, B. Li, A. Magomedov, H. Hempel, P. Caprioglio, J. A. Márquez, A. B. Morales Vilches, E. Kasparavicius, J. A. Smith, N. Phung, D. Menzel, M. Grischek, L. Kegelmann, D. Skroblin, C. Gollwitzer, T. Malinauskas, M. Jošt, G. Matič, B. Rech, R. Schlatmann, M. Topič, L. Korte, A. Abate, B. Stannowski, D. Neher, M. Stolterfoht, T. Unold, V. Getautis, S. Albrecht, *Science* **2020**, *370*, 1300.
[33] H. Köbler, S. Neubert, M. Jankovec, B. Glazar, M. Haase, C. Hilbert, M. Topic, B. Rech, A. Abate, *Energy Technol.* **2022**, *10*, 2200234.
[34] M. Khenkin, H. Köbler, M. Remec, R. Roy, U. Erdil, J. Li, N. Phung, G. Adwan, G. Paramasivam, Q. Emery, E. Unger, R. Schlatmann, C. Ulbrich, A. Abate, *Energy Environ. Sci.* **2023**, *17*, 602.
[35] S. Arrhenius, *Z. Für Phys. Chem.* **1889**, *4*, 96.
[36] J. Ascencio-Vásquez, K. Brecl, M. Topič, *Sol. Energy* **2019**, *191*, 672.
[37] M. Sengupta, Y. Xie, A. Lopez, A. Habte, G. Maclaurin, J. Shelby, *Renew. Sustain. Energy Rev.* **2018**, *89*, 51.